Kinetic Modeling of Aggregation and Gel Formation in Quiescent Dispersions of Polymer Colloids

*Marco Lattuada, Peter Sandkühler, Hua Wu, Jan Sefcik, Massimo Morbidelli**

Institute of Chemical- and Bioengineering, Swiss Federal Institute of Technology, ETH-Hönggerberg, CH-8093 Zürich, Switzerland
E-mail: morbidelli@tech.chem.ethz.ch

Summary:
In this work, a methodology suitable for the description of aggregation and gel formation processes of polymeric colloidal dispersions in quiescent conditions is presented. The modeling of aggregation is based on the use of populations balance equations to describe the time evolution of the aggregate distribution. Monte-Carlo simulations are used to generate the structural properties of individual aggregates, which are necessary to compute the average radius of gyration and hydrodynamic radius that are compared to the values measured using light scattering. The agreement between model predictions and measured sizes is good in both diffusion-limited and reaction-limited conditions. For the description of progress toward gel formation, the cumulatively occupied volume, a measure of the fraction of space occupied by the clusters, is defined. Due to the fractal nature of clusters, during the aggregation the system can reach a condition of space filling, after which the formation of gel is a result of the interconnection of the clusters. It is found that in diffusion-limited conditions the interconnection step is much faster than the preceding aggregation, while in reaction-limited conditions the aggregation and the interconnection are of comparable duration.

Keywords: aggregate structure; aggregation; gel formation; kinetics; light scattering

Introduction

Emulsion polymerization processes typically yield latexes of polymer particles in the submicron size range at solid volume fractions of 10-50% [1]. For many applications a separation of polymer and aqueous phase is necessary and this is achieved by aggregating the primary particles into larger aggregate or gel structures. These can be separated in subsequent units from the aqueous phase by filtration or sedimentation. Due to the high solid volume fractions aggregation is often accompanied by gel formation after the latex has been destabilized. In order to better understand and design the process of aggregation and subsequent gel formation this work describes the tools

 DOI: 10.1002/masy.200450224

for the development of quantitative kinetic models for these processes. We focus herein on irreversible aggregation characterized by the domination of strong short-range attractive forces between the particles which comprise the aggregates. The approach to account for the interactions between primary particles is explained in the following section on colloidal stability. In order to characterize the open structure of the aggregates we use Monte-Carlo simulations and present a model that describes accurately the different aggregate structures developing in stagnant dispersions (no shear). This open structure is also the reason for the occurrence of gel formation. Subsequently we introduce the kinetic equations within the framework of population balance equations (PBE) that are used to describe the time evolution of the complete cluster mass distribution (CMD). In order to validate this aggregation model we calculate from the CMD the average hydrodynamic and gyration radii making use of the structure models obtained from the Monte-Carlo simulations. These calculated radii are compared to light scattering measurements of the same quantities. The aggregation model is shown to be accurate for various initial solid volume fractions and rates of aggregation. In the remaining part of this work we analyze the gel formation process. We relate the gel formation kinetics to the aggregation kinetics preceding it and show that it is reasonable to treat the complete gel formation as a two step process. In this context, we highlight what is already understood and which part of the gel formation kinetics still requires further investigation.

Colloidal Stability

Most lateces that are intended to be aggregated are initially stabilized by repulsive electrostatic potentials. Either ionic surfactants are adsorbed or sulfonated or carboxylated copolymers are incorporated on the surface of the polymer particles to provide the stability against coalescence or aggregation during the polymerization process. This type of stabilization has the advantage over steric stabilization to be more easily overcome when aggregation is initiated. Aggregation is achieved by addition of salt or acidic solutions, which increase the ionic strength of the liquid phase and shield the electrostatic repulsion. The attractive van-der-Waals forces can then prevail and cause aggregation. This interplay of forces is often characterized within the well known DLVO theory by the total interaction potential V_T which is expressed as the sum of the attractive van-der-Waals potential V_A and the electrostatic repulsive potential V_R. Here we refer to the literature for the corresponding equations [2-5]. V_T can be used to calculate the colloid stability

ratio W by [3]

$$W = \frac{K_B}{K_{11}} = 2a \int_{2a}^{\infty} \frac{\exp(V_T / k_B T)}{G(r) r^2} dr \qquad (1)$$

where $G(r)$ accounts for the hydrodynamic interactions, a is the primary particle radius, k_B the Boltzmann constant, T the absolute temperature and r the center to center distance between approaching particles. In equation (1) we relate W also to the measured aggregation rate constant of primary particles K_{11}, while $K_B = 8k_BT/3\eta$ is the Brownian aggregation rate constant resulting from complete destabilization corresponding to diffusion-limited aggregation (DLCA). The ratio between K_B/K_{11} quantifies the extent of destabilization and consequently the actual reduced aggregation rate due to the remaining small repulsive interactions. Here, particles and aggregates undergo several collisions before forming a new aggregate and this corresponds to reaction-limited aggregation (RLCA). It was found that for dispersions with a high surface charge density, typical for latexes of interest here, the DLVO theory does not provide reliable values of W but can be wrong by an order of magnitude [5]. Furthermore, it turns out that equation (1) is extremely sensitive to small uncertainties in the values of the particle surface charge or surface potential. Therefore we use the stability ratio as defined in equation (1) and rely ultimately on direct measurements of the actual aggregation rate constant K_{11}, which are described elsewhere [6]. W and K_{11} will be used later in the formulation of the matrix of the aggregation rate constants K_{ij} for aggregates of dimensionless mass i and j.

Structure of Aggregates by Monte Carlo Simulations

In order to describe quantitatively the kinetics of aggregation and gel formation in quiescent conditions, one needs some information about the structure of individual aggregates formed under DLCA and RLCA conditions. The average structural properties of individual aggregates can be determined either experimentally or computationally [7-10]. The experimental procedure requires usually the visual examination of two-dimensional electron micrographs of hundreds of real clusters with the same mass to reconstruct their three dimensional structure [7,8]. This is a very cumbersome procedure, which furthermore requires substantial manipulation of the samples, during which the cluster structure can be altered. On the other hand, computational methods like Monte-Carlo (MC) simulations allow one to generate thousand of clusters with the same mass, and enable one to calculate easily all their structural properties through the knowledge of the

coordinates of the particles constituting the clusters [9]. Therefore, in this work we have used MC simulations. These are based on cluster-cluster aggregation algorithms that imitate the real aggregation process in a very simplified manner by neglecting most of its physical complexity. In the case of DLCA and RLCA process, all the physics of aggregation is lumped into the assumptions that clusters move randomly according to Brownian motion rules, with a diffusion coefficient inversely proportional to their size, and that whenever two clusters collide, they form a new cluster with a sticking probability equal to *1* under DLCA conditions, and equal to *0.001* under RLCA conditions.

It turns out that, in order to obtain the average properties of clusters of a given mass, it is convenient to compute the cluster particle-particle correlation function *g(r)* [9]. This function counts the average number of particles per unit volume at a distance *r* from each particle in the cluster. The shape of the particle-particle correlation function has been analyzed in detail, and it has been found that there are three different regions into which it can be divided. First, the *g(r)* function has a peak at a distance *r=2a*, corresponding to the first coordination shell of particles surrounding each particle in a cluster. Then, in the range of distances *2a<r<4a*, corresponding to the second coordination shell, the particle-particle correlation function shows a behavior that can be described using a power law function. Finally, for *r>4a*, the *g(r)* function shows a typical fractal scaling followed by a sharp cut-off, accounting for the finite size of the cluster. In synthesis, the particle-particle correlation function can be represented by the following piece-wise equation [9]:

$$g(r)=\begin{cases} N_{nn}\dfrac{\delta(r-2a)}{4\pi(2a)^2} \\ Ar^{b} \\ cr^{d_f-3}\exp\left(-\left(\dfrac{r}{\xi}\right)^{\gamma}\right) \end{cases} \quad for \begin{cases} r=2a \\ 2a<r<4a \\ r>4a \end{cases} \tag{2}$$

In equation (2), d_f is the cluster fractal dimension, N_{nn} is the number of average nearest neighbor particles per particle, A and b are fitting parameters, ξ is the cluster cut off size, γ is the cut-off exponent and c a normalization constant. The parameters appearing in equation (2) as functions of the cluster mass tend to reach asymptotic values as the cluster mass becomes sufficiently large (usually 50 to 60 particles per clusters are enough), indicating when the self similarity, the typical

fingerprint of the fractal nature of the clusters, starts to apply. A typical example of a particle-particle correlation function computed through Monte-Carlo simulations is shown in figure 1a for a DLCA cluster with mass equal to *30* particles, together with the fit obtained using equation (2). The advantage of having a reliable model for the particle-particle correlation function is that the *g(r)* function allows one to compute the most important cluster structural properties needed in the investigation of colloidal aggregation. First, the scattering structure factor *S(q)* can be calculated, since it is simply the Fourier transform of the particle-particle correlation function [9]:

$$S(q) = \frac{1}{i}\left(1 + 4\pi \int_0^\infty g(r) r^2 \frac{\sin(qr)}{qr} dr\right), \tag{3}$$

where q is the scattering wave vector modulus, related to the scattering angle θ at which the scattered radiation is detected, and i is the number of particles in the cluster. Typical shapes of structure factors of DLCA clusters with masses equal to 30, 60 and 100 particles are shown in figure 1b. In addition to the scattering structure factor, two different sizes that depend on the geometrical arrangement of the particles in the cluster can be also determined: the radius of gyration R_g and the hydrodynamic radius R_h. The radius of gyration, which depends on the moment of inertia of the cluster computed with respect to its center of mass, is simply given by the following expression [9,11]:

$$R_g^2 = R_{g,p}^2 + \frac{4\pi}{2i} \int_0^\infty g(r) r^4 dr, \tag{4}$$

where $R_{g,p}$ is the primary particle radius of gyration. Since the hydrodynamic radius is the radius of the equivalent sphere that has the same drag coefficient as the cluster, it is clear that the estimation of R_h is by far not as simple as that of R_g, because it requires to estimate the interactions of a cluster with a fluid in the viscous regime. Even though a rigorous expression for R_h cannot be derived, a good estimate of the hydrodynamic radius can be obtained by applying the Kirkwood-Riseman theory. This approach assumes that the total drag force acting on a cluster can be computed if the drag force experienced by its average particle is known. This last quantity strongly depends on the structural arrangement of all the other particles in the cluster. The calculations lead to the following expression for R_h [10]:

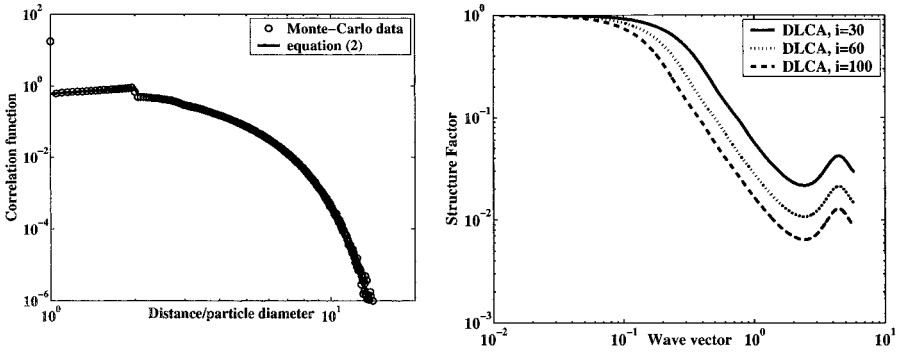

Figure 1. Structural properties resulting from the MC simulations. (a) Particle-particle correlation function for a DLCA cluster with mass equal to 30 particles (symbols) and the corresponding fitting using equation (2) (line). (b) Structure factors for three DLCA clusters with masses 30 (continuous line), 60 (dotted line) and 100 particles (dashed line).

$$R_h = \frac{ia}{1+4\pi a\int_0^{\infty} g(r)rdr} \tag{5}$$

In synthesis, MC simulations allow one to compute the particle density correlation function of clusters with a given mass, from which the most valuable information about size and scattering properties of the cluster can be derived.

Aggregation Kinetics

During the aggregation process, a distribution of cluster masses (CMD) develops due to the random nature of the process. The population balance equations (PBE) describing the formation and disappearance of the number N_k of aggregates per unit volume having mass k due to aggregation are given by [3,4,6]

$$\frac{dN_k}{dt} = \frac{1}{2}\sum_{i+j=k} K_{ij}N_iN_j - \sum_i K_{ik}N_iN_k\,, \tag{6}$$

where the first term on the right-hand side of equation (6) accounts for the formation of aggregates of mass k from two smaller ones and the second term for the loss of these aggregates due to the combination with all other aggregates. The matrix of the aggregation rate constant K_{ij} is specified by the following equations [4,6]

$$K_{ij} = K_B W^{-1} B_{ij} P_{ij} \quad \text{with}$$
$$B_{ij} = \left(i^{-1/d_f} + j^{-1/d_f}\right)\left(i^{1/d_f} + j^{1/d_f}\right) \tag{7}$$
$$P_{ij} = (ij)^{\lambda}$$

K_B and W have been introduced above. The matrix B_{ij} accounts for the size dependence of the cluster mobility (diffusion coefficient) and its collision cross section. The matrix P_{ij} is necessary for RLCA, where the aggregation rate increases with the cluster size. A crossover to DLCA is expected once the product of $W^{-1}P_{ij}$ exceeds unity, after this it is set to unity so that aggregation proceeds at the highest possible rate, *i.e.* the DLCA rate. The parameter l quantifies how fast the reactivity of RLCA clusters grows with their size and typically takes values in the range (0;0.5), as discussed in detail below.

In order to calculate the average hydrodynamic and gyration radii from the calculated CMD we have to use the correct averages of the CMD for each of the radii. The average radius of gyration is given by [4,6,12,13]

$$\left\langle R_g \right\rangle^2 = \frac{\sum_i i^2 N_i R_{g,i}^2}{\sum_i i^2 N_i}. \tag{8}$$

In addition to being an average of the CMD, the measured hydrodynamic radius of fractal aggregates depends on the scattering wave vector q. This dependence is due to the contribution of rotational diffusion of fractal aggregates to the measured light scattering signal, *i.e.* the autocorrelation function [12,13]. The calculation of the average hydrodynamic radius is then achieved by averaging over the CMD and introducing an effective hydrodynamic radius $R_{h,i,eff}$ which accounts for the contribution of rotational diffusion [4,6,12-14]:

$$\left\langle R_{h,eff} \right\rangle = \frac{\sum_i i^2 N_i S_i(q)}{\sum_i i^2 N_i S_i(q) R_{h,i,eff}^{-1}} \tag{9}$$

$$\frac{R_{h,i}}{R_{h,i,eff}} = 1 + \frac{1}{2\beta^2}\left(1 + \frac{3\partial \ln S_i(q)}{\partial (qR_{g,i})^2}\right). \tag{10}$$

Equation (9) performs the average over the CMD by using an effective hydrodynamic radius that is calculated by equation (10) accounting for rotational diffusion. In equation (10) we see that the contribution of rotational diffusion depends on the aggregate structure factor, the scattering wave

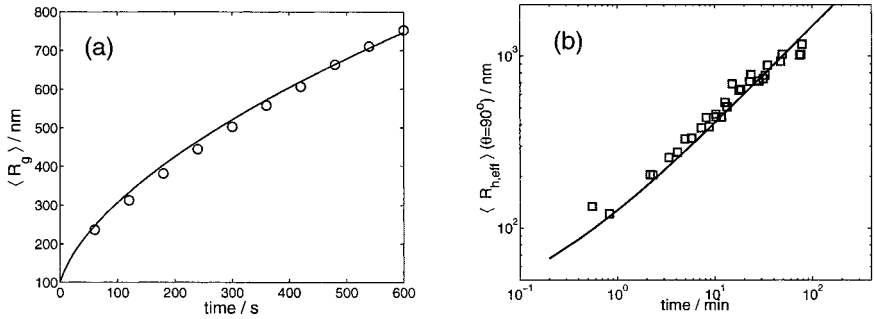

Figure 2. Comparison between experimental (symbols) and simulation (lines) results for DLCA. (a) Time evolution of the radius of gyration for carboxylated polystyrene (salt concentration: $CaCl_2$, 0.2mol/l + HNO_3, 0.01mol/l). Volume fraction and particle radius: $\phi_0=2.5\text{x}10^{-5}$ and a=250nm [9]. (b) Time evolution of the hydrodynamic radius measured at an angle of 90° for polystyrene stabilized by anionic surfactant (SDS) (salt concentration: $MgCl_2$, 0.1mol/l). Volume fraction and particle radius: $\phi_0=1.0\text{x}10^{-5}$ and a=35nm [15].

vector q and the size of the aggregate, while β is the ratio between the hydrodynamic radius and the radius of gyration of a cluster with mass i discussed in the previous section.

In order to validate the aggregation model we compare the model predictions with experimental data of $\langle R_g \rangle$ and $\langle R_{h,eff} \rangle$ for several polymer colloids, both in the DLCA and in the RLCA regime. We first discuss DLCA, where the matrix of rate constants is given by $K_{ij}=K_B W^{-1} B_{ij}$. Since the electrostatic interactions are completely screened in DLCA, W is used to account for hydrodynamic interactions and takes values in the range [0.5;2]. In figure 2a we compare the time evolution of the experimentally determined radius of gyration with the model predictions for a polystyrene latex with primary particles of *a=125nm*. For this system, W has been adjusted to 2 in order to achieve a good fit of the data [9]. For smaller polystyrene particles *(a=35nm)* the experimentally measured hydrodynamic radius (at 90°) agrees well with the model calculation, as shown in figure 2b. Here, W has been adjusted to 0.5 [15]. It is worth mentioning that the model describes well also other colloidal systems such as gold and silica and is capable to resolve the angle dependence of the effective hydrodynamic radius [4].

In RLCA the full aggregation rate constant is used as given by equation (7). Two parameters appear in the model: W and λ. As mentioned above, W is determined independently from the rate of aggregation of primary particles, and therefore the only fitting parameter left is λ.

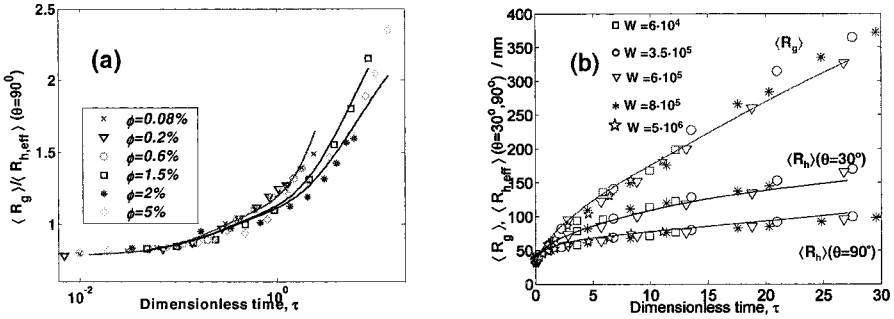

Figure 3. Comparison between experimental (symbols) and simulation (lines) results for RLCA using a MFA polymer colloid with a=37.5nm. (a) Time evolution of the ratio between the radius of gyration and the hydrodynamic radius at 90° for several different volume fractions [6]. (b) Time evolution of the hydrodynamic radius measured at angles of 30° and 90° and the radius of gyration at ϕ_0=0.05 for several different salt concentrations and stability ratios [16].

In order to better compare experimental data obtained for aggregating systems with significantly different values of W and particle volume fractions, it is convenient to introduce a dimensionless time τ, defined by the following expression [6]:

$$\tau = \frac{N_0 K_B t}{W}, \tag{11}$$

where N_0 is the initial number of primary particles in the system and t is the real time. In the framework of the developed aggregation model, this dimensionless time incorporates all the information concerning the initial particle volume fraction and the stability of particles. By rewriting the population balance equations in terms of this dimensionless time τ, and normalizing the number concentration of aggregates using the initial number of particles N_0, it is in fact found that in the model in dimensionless form the only parameter, λ, is present. This implies that, if this parameter was independent of the aggregation conditions, all the data points collected at different experimental conditions should collapse on a single master curve.

In figure 3a we show experimental data of the ratio $\langle R_g \rangle$ and $\langle R_{h,eff} \rangle$ for several different volume fractions ranging from $\phi_0=8.0\times10^{-4}$ *to* $\phi_0=0.05$, as a function of the dimensionless time τ. It turns out that in order to obtain good agreement with the experimental data, λ has to be decreased as the solid volume fraction increases. The values determined range from $\lambda=0.4$ for dilute

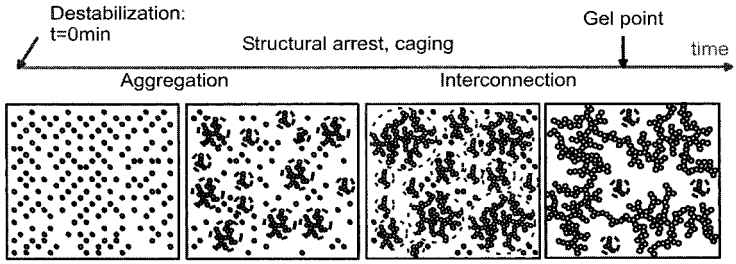

Figure 4. Schematic of the aggregation and gel formation process.

conditions to $\lambda=0.11$ for $\phi_0>0.02$. The origin of this dependence is not clear yet, but could be related to hydrodynamic interactions between aggregates [6] or to effects of interaction potentials which are a function of ϕ_0 due to complex surfactant adsorption equilibria. At the highest volume fraction investigated in figure 3a ($\phi_0>0.02$), further aggregation experiments were performed at various salt concentrations and thus different stability ratios. The results together with the model calculations are shown in figure 3b [16]. In this case a constant value of $\lambda=0.11$ has been found for all five stability ratios investigated, thus indicating that for RLCA λ is not affected by the stability ratio or the rate of aggregation.

Gel Formation Kinetics

Aggregation processes at volume fractions of $\phi_0>0.01$ almost ubiquitously result in the formation of a solid phase. This colloidal gel is a network structure formed by the fractal aggregates that have grown to such an extent that they occupy the total volume of the dispersion. In order to form the network the aggregates have to interconnect with each other. This interconnection step is quite different from the preceding aggregation step in that aggregates do not diffuse randomly but directly experience their nearest neighbors. Therefore they have to move cooperatively in order to rearrange their spatial configuration substantially which becomes increasingly unlikely on approach to the gel point. In figure 4 is shown a schematic of the gel formation process, where we distinguish between the aggregation and the interconnection step. The aggregation step for

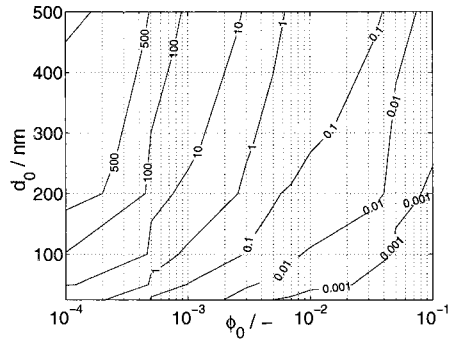

Figure 5. Calculation of the time (in minutes) it takes in DLCA to reach $\phi^*=0.5$. The times are given as contour lines in a plane of the initial conditions: solid volume fraction ϕ_0 and primary particle diameter d_0.

either DLCA or RLCA conditions is well described by the population balance model (6). In order to identify when aggregation crosses over to interconnection, a cumulatively occupied volume $\phi(t)$ can be defined [15,17,18].

$$\phi(t) = \sum_i v_i N_i \tag{12}$$

where $v_i = 4\pi/3R_i^3$ is the volume of the enclosing sphere with radius R_i, which can be related to the radius of gyration of an aggregate by $R_i=R_{g,i}/(d_f/(d_f+2))^{0.5}$, while $\phi(t)$ quantifies the increasing space (or volume fraction) occupied by the growing clusters. Once this reaches a value of $\phi^*(t)\sim 0.5$ the aggregates cannot freely move and the corresponding time t_a is defined as the arrest time of the aggregation step [15]. After reaching this value, the aggregation mechanism crosses over to the interconnection one. This picture has been established by Monte Carlo simulations of diffusion limited cluster-cluster aggregation where the interconnection step has been found to show features characteristic of percolation [17,18].

In the analysis of the kinetics of gel formation it is useful to distinguish between DLCA and RLCA. In DLCA, every collision between particles and clusters results in a new aggregate. Once during the aggregation process $\phi^*(t)\sim 0.5$ is reached, the aggregates are in close vicinity to each other and start to interconnect. This interconnection process is very fast for two reasons: the characteristic CMD of DLCA is rather monodisperse and therefore all aggregates experience

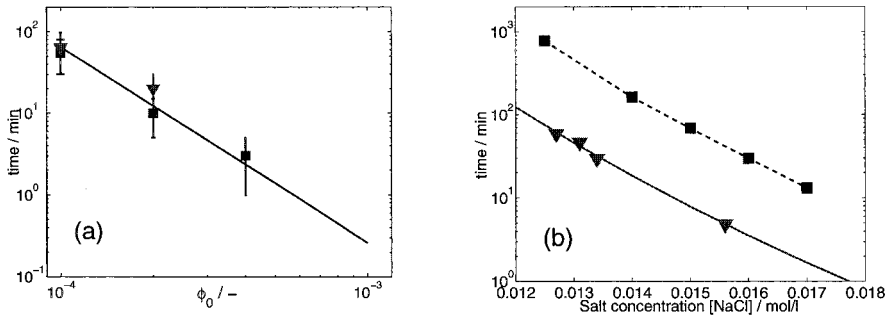

Figure 6. (a) Gel formation (squares) and arrest times (triangles) for DLCA gel formation in dilute conditions [15]. The full lines are model calculations of the arrest times as discussed in the text. (b) Gel formation and arrest times in RLCA for MFA colloid [16]. The broken line is a guide to the eye.

approximately the same environment and are on average separated by the same short distance; and almost any short distance diffusion of such an aggregate or its subunits attaches this aggregate to its neighbors due to the absence of repulsion barrier characteristic of DLCA conditions. This view is confirmed by experiments performed on the same polystyrene colloid discussed in figure 3b. In figure 6a are shown the gel formation times and the arrest times as a function of solid volume fraction. Both times are almost overlapping within the experimental error and this confirms that the interconnection step is apparently extremely short compared to the aggregation step. A simple model for the interconnection time has been proposed based on the characteristic distance between aggregates at the arrest time and their apparent diffusion coefficient [15]. It has been further argued that in the case of DLCA, all the interconnection events occur almost simultaneously. The model results compare well to the observed very short interconnection times. Through this model we can calculate the arrest times as a good estimate of the actual gel time for several initial conditions of solid volume fraction ϕ_0 and primary particle diameter d_0. The results are summarized in the contour plot in figure 5, where the arrest times for different initial conditions are plotted in the phase plane ϕ_0-d_0. It is seen that the DLCA kinetics becomes extremely fast for small particles at high volume fractions, which are typically of interest in industrial applications.

In RLCA, on the other hand, it is possible, by tuning salt concentration and particle volume fraction, to adjust the aggregation rate such that we can observe the gel formation process over

the whole range of the diagram in figure 5. An example of such a gel formation process is given in figure 6b, where the gel formation and arrest times for the aforementioned MFA system are shown. The volume fraction and particle size are the same as in figure 3b and the data therein actually represent the aggregation step preceding the gel formation [16]. In this case the interconnection time, *i.e.* the time required after the crowding of the system for the actual formation of the network is not negligible. This is likely due to the low reactivity of aggregates in RLCA and their reduced diffusivity, which is hindered by the surrounding aggregates of various sizes. Currently, no kinetic model is available to predict the gel formation time in RLCA at high volume fractions. Such models are of interest to better understand and design gel formation processes in industrial applications.

Conclusions

In this work, we have outlined a methodology for the modeling of aggregation and gel formation kinetics of polymer colloidal dispersions in quiescent conditions, both in diffusion-limited and reaction-limited conditions. It turns out that the description of aggregation and gel formation kinetics requires an appropriate combination of experimental measurements and of modeling tools. The whole description is based on the use of population balance equation to model the time evolution of the cluster mass distribution. In order to apply effectively the PBE, information about the structure of individual aggregates and about the stability of particles is required. The stability of particles is described by the Fuchs stability ratio which is estimated from the measured rate of aggregation of primary particles to form doublets. In order to obtain reliable information about the structure of aggregates, off-lattice MC simulations have been performed to generate thousands of clusters with a given mass, in both DLCA and RLCA conditions, so that their average properties could be investigated. In particular, the particle-particle correlation function of clusters has been computed, from which the fractal dimension, the scattering structure factor, the radius of gyration and the hydrodynamic radius have been estimated. These individual properties have been combined with the cluster mass distribution computed through the PBEs, so that the time evolution of the computed average radius of gyration and hydrodynamic radius can be compared with the experimental values measured using light scattering. The results show that a good agreement between model predictions and experimental data is achieved, under both RCLA and DLCA conditions.

On the other hand, the formation of a gel can be described as a two step process depending on the volume cumulatively occupied by the population of aggregates, which represents the fraction of space occupied by the fractal clusters. As a result of the low fractal dimension of the clusters formed during the aggregation, the cumulatively occupied volume increases, leading to a condition of space filling where the threshold of volume fraction equal to 0.5 is reached. At this point, the gel formation is not a free diffusion process anymore, but switches to a mechanism, possibly percolation, where the clusters interconnect to form the final gel network. In DLCA conditions experiments and simulations suggest that the interconnection step is much faster than the aggregation process, and therefore the time required for the cluster to reach an occupied volume index of 0.5 is a good estimate of the gel time. In RLCA conditions, on the other hand, it seems that the gel time is significantly longer than the time required to reach a cumulatively occupied volume fraction of $\phi^*=0.5$. The kinetic description of this second step is so far only qualitative. It is not yet clear, how the gel structure evolves from the distribution of aggregates with their individual structure and how the kinetics of the transition is influenced by factors like particle interaction potentials and reduced diffusivity of aggregates after passing the arrest time.

Acknowledgments

We thank Eleonora Bonanomi for the calculations shown in figure 5. This work was supported by the Swiss National Science Foundation (NSF), under Grant No. 2000-061883.

[1] R.B. Fitch, Polymer colloids: a comprehensive introduction, Academic press, San Diego (1997).
[2] J. Sefcik, M. Verduyn, G. Storti and M. Morbidelli, Langmuir, **19**, 4778 (2003).
[3] S. Melis, M. Verduyn, G. Storti, M. Morbidelli and J. Baldyga, AIChE Journal, **45**, 1383 (1999).
[4] P. Sandkühler, J. Sefcik, M. Lattuada, H. Wu and M. Morbidelli, AIChE Journal, **49**, 1542 (2003).
[5] S.H. Behrens, D.I. Christl, R. Emmerzael, P. Schurtenberger and M. Borkovec, Langmuir, **16**, 2566 (2000).
[6] M. Lattuada, P. Sandkühler, H. Wu, J. Sefcik and M. Morbidelli, Adv. Colloid Interface Sci., **103**, 33-56 (2003).
[7] G.C. Bushell, Y.D. Yan, D. Woodfield, J. Raper, and R. Amal, Adv. Colloid Interface Sci., **95**, 1-50 (2002).
[8] J. Cai, N. Lu, and C.M. Sorensen, Langmuir, **9**, 2861-2867 (1993).
[9] M. Lattuada, H. Wu and M. Morbidelli, J. Colloid Interface Sci., in press.
[10] M. Lattuada, H. Wu and M. Morbidelli, J. Colloid Interface Sci., in press.
[11] P. Lindner and Th. Zemb, *Neutrons, X-rays and Light: Scattering Methods Applied to Soft Condensed Matter* Elsevier (2002)
[12] M.Y. Lin, H.M. Lindsay, D.A. Weitz, R.C. Ball, R. Klein and P. Meakin, Phys. Rev. A **41**, 2005 (1990).
[13] M.Y. Lin, H.M. Lindsay, D.A. Weitz, R.C. Ball, R. Klein and P. Meakin., J. Phys.: Condens. Matter **2**, 3093 (1990).
[14] M.Y. Lin, H.M. Lindsay, D.A. Weitz, R.C. Ball, R. Klein and P. Meakin, Proc. R. Soc. Lond. A **423**, 71 (1989)
[15] P. Sandkühler, J. Sefcik and M. Morbidelli, Adv. Colloid Interface Sci., in press.
[16] P. Sandkühler, J. Sefcik and M. Morbidelli, (2003), in preparation.
[17] J.C. Gimel, D. Durand and T. Nicolai, Phys. Rev. B **51**, 11348 (1995).
[18] J.C. Gimel, D. Durand and T. Nicolai, J. Sol-Gel Sci. Techn. **15**, 129 (1999).